Anomalous mechanics of Zn^{2+}-modified fibrin networks

Jing Xia[a], Li-Heng Cai[a,b], Huayin Wu[a], Frederick C. MacKintosh[c,d,e,f], and David A. Weitz[a,g,1]

[a]John A. Paulson School of Engineering and Applied Sciences, Harvard University, Cambridge, MA 02138; [b]Department of Materials Science and Engineering, University of Virginia, Charlottesville, VA 22904; [c]Department of Chemical and Biomolecular Engineering, Rice University, Houston, TX 77005; [d]Center for Theoretical Biological Physics, Rice University, Houston, TX 77030; [e]Department of Chemistry and Physics, Rice University, Houston, TX 77005; [f]Department of Astronomy, Rice University, Houston, TX 77005; and [g]Department of Physics, Harvard University, Cambridge, MA 02138

Edited by Tom C. Lubensky, University of Pennsylvania, Philadelphia, PA, and approved January 4, 2021 (received for review October 3, 2020)

Fibrin is the main component of blood clots. The mechanical properties of fibrin are therefore of critical importance in successful hemostasis. One of the divalent cations released by platelets during hemostasis is Zn^{2+}; however, its effect on the network structure of fibrin gels and on the resultant mechanical properties remains poorly understood. Here, by combining mechanical measurements with three-dimensional confocal microscopy imaging, we show that Zn^{2+} can tune the fibrin network structure and alter its mechanical properties. In the presence of Zn^{2+}, fibrin protofibrils form large bundles that cause a coarsening of the fibrin network due to an increase in fiber diameter and reduction of the total fiber length. We further show that the protofibrils in these bundles are loosely coupled to one another, which results in a decrease of the elastic modulus with increasing Zn^{2+} concentrations. We explore the elastic properties of these networks at both low and high stress: At low stress, the elasticity originates from pulling the thermal slack out of the network, and this is consistent with the thermal bending of the fibers. By contrast, at high stress, the elasticity exhibits a common master curve consistent with the stretching of individual protofibrils. These results show that the mechanics of a fibrin network are closely correlated with its microscopic structure and inform our understanding of the structure and physical mechanisms leading to defective or excessive clot stiffness.

fibrin gel | Zn^{2+} | bundle | three-dimensional networks | mechanics

Fibrin is the major component of blood clots, which stops bleeding from wound sites of blood vessels (1, 2). Upon injury, blood clots form when fibrinogen is converted to fibrin monomers, which polymerize into a fibrous gel that can withstand the pressure from the flowing blood and can therefore stop further blood loss (3–6). The mechanical properties of fibrin gels determine the performance of blood clots during hemostasis (7, 8): They must be mechanically strong enough to withstand the pressure of arterial blood; otherwise, the clots will not stop the loss of blood (9). They must also be strong enough to withstand the viscous forces; otherwise, parts of the gel may break off and be carried in the blood, where they may lodge in a vessel in the brain or the heart, which can cause a stroke or a heart attack (10, 11). The pressure of the blood is not constant; instead, it varies over a wide range, depending on locations in the body (12). Thus, the mechanical response of fibrin gels to the extent of pressure, or stress, is also crucial in determining the success of hemostasis. Fibrin gels exhibit a stress-dependent mechanical response (13, 14), similar to the gel networks formed from many other biopolymers, including actin, vimentin, neurofilaments, and collagen (15). Under small stresses, fibrin gels exhibit linear elasticity with the applied stress linearly proportional to the strain. By contrast, under large stresses, fibrin gels exhibit stress stiffening with the applied stress increasing nonlinearly with the strain.

The mechanical property of the fibrin gel depends on the concentration of fibrinogen, as well as on many other factors (16–20). For example, the stiffness increases with the concentration of divalent cations such as Ca^{2+}, which effectively acts as an additional cross-linker leading to the formation of a network from the filaments (17). Intriguingly, however, another divalent cation, Zn^{2+}, seems to have the opposite effect: The stiffness of clots decreases with increasing concentration of Zn^{2+} (17); furthermore, the permeability of clots increases with increasing concentration of Zn^{2+} (21). This has important consequences as Zn^{2+}, the second most abundant trace metal ion in the body (22, 23), is released from activated platelets during hemostasis, which can locally change its concentration (18, 19). Furthermore, Zn^{2+} deficiency in the blood is associated with abnormal blood clotting (24, 25). Nevertheless, the origin of effects and the impact of Zn^{2+} on the structure and properties of blood clots remain unclear. The effect of the addition of Zn^{2+} is correlated with the formation of a sparser network in the fibrin gel, as observed with two-dimensional (2D) scanning electron microscopy (SEM) (21). However, the observed network morphology is likely altered by drying during sample preparation (26), and 2D images cannot provide complete information about the network morphology; thus, the effects of the addition of Zn^{2+} on the three-dimensional (3D) structure of the gel network remains unknown. To understand the origin of the unusual decrease in stiffness upon addition of Zn^{2+}, the mechanics of the fibrin gel must be correlated with Zn^{2+}-induced changes in its network structure and properties.

In this paper, we correlate the 3D structure of fibrin networks formed in the presence of Zn^{2+} with their mechanical properties to determine the consequences of the structure on the mechanical properties of fibrin gels. We use confocal microscopy to probe the 3D structure of the gel in its hydrated state and rheological measurements to probe its mechanics. We focus on the fully gelled structure, where the network has reached its steady state; thus, we can measure the confocal microscopy and rheology on separate samples whose structure and properties will nevertheless be identical. We find that as the Zn^{2+} concentration increases, the diameter of the fibrin fibers in the gel becomes measurably thicker

Significance

Fibrin forms a three-dimensional network in blood clots during hemostasis that must be strong enough to stop bleeding yet flexible enough to withstand pressure variations of arterial flow. During clotting, activated platelets release Zn^{2+} whose effect on the structure and mechanics of fibrin gels is poorly understood. We show that Zn^{2+} unexpectedly reduces fibrin gel stiffness even though it induces bundling that coarsens the network. This results from weak interactions between the fibrils that make up the bundle, leading to a loose coupling that results in a softer network. These results provide important insight into the impact of Zn^{2+} on the behavior of blood clots and represent a different class of network that becomes weaker even with increasing bundle thickness.

Author contributions: J.X., F.C.M., and D.A.W. designed research; J.X. performed research; J.X. analyzed data; and J.X., L.-H.C., H.W., F.C.M., and D.A.W. wrote the paper.

The authors declare no competing interest.

This article is a PNAS Direct Submission.

[1]To whom correspondence may be addressed. Email: weitz@seas.harvard.edu.

This article contains supporting information online at https://www.pnas.org/lookup/suppl/doi:10.1073/pnas.2020541118/-/DCSupplemental.

Published March 1, 2021.

while the total length of the fibrin fibers in the network becomes shorter; these results are explained by an increase in the number of protofibrils that are bundled together to form each fiber in the network. Bulk rheological measurements of the small-stress, linear elastic modulus of these gels are consistent with this structural packing of the protofibrils in the fibers; moreover, these results show that the protofibrils are not strongly coupled to one another in the fibers, which explains why the network becomes softer as the concentration of Zn^{2+} increases. At intermediate applied stresses, pronounced stress-stiffening is observed. Remarkably, at large applied stresses, the data from all the networks can be scaled together, indicating that the elastic modulus of the fibrin gels results from stretching of the individual fibrin protofibril that forms the bundles that make up the network. These results show that the mechanics of a fibrin network is correlated with its microscopic structure and provide important insight into the effect of Zn^{2+} on the mechanics of blood clots.

Results and Discussion

Morphology Quantification of Fibrin Networks. Fibrin gels are networks made up of bundled fibrin protofibrils that are cross-linked by factor XIII (FXIII). Protofibrils are formed when thrombin, an enzyme in the blood, cleaves fibrinogen, the fibrin monomer, which allows them to assemble into two-stranded protofibrils (1). The protofibrils are further bundled in a parallel manner to form fibrin fibers, which form a 3D network structure, as shown in Fig. 1*A*. To investigate the network structure of Zn^{2+}-modified fibrin networks, we polymerize fibrin gels in the presence of different Zn^{2+} and fibrinogen concentrations. We fluorescently label fibrinogen with tetramethylrhodamine (TRITC), and mix labeled and unlabeled fibrinogen in a 1:6 ratio. The mixed fibrinogen solution is incubated with $ZnCl_2$ in a tricine buffer system for 5 min. The mixtures are loaded into an imaging chamber composed of two 22-mm-diameter #1.5-thickness coverslips with a 1-mm-thick spacer, and polymerization is initiated by incubating with 1 NIH units/mL human α-thrombin at 25 °C. The polymerized fibrin gels are imaged using a confocal microscope equipped with a 63×/1.2 numerical aperture (N.A.) water immersion objective. Optical cross-sections of the fibrin gels are recorded at a *z*-axis interval of 0.1 μm to obtain 3D images of fibrin networks, as shown in Fig. 1*B*. Movies of rotating 3D confocal images of fibrin networks are included as Movies S1 and S2. The 3D images are further analyzed to extract the skeleton of the fibrin network using commercial image-processing software (Amira), as shown in Fig. 1*C*. Movies of rotating skeletons of fibrin networks are included as Movies S3 and S4. The extracted skeletons of the networks are used

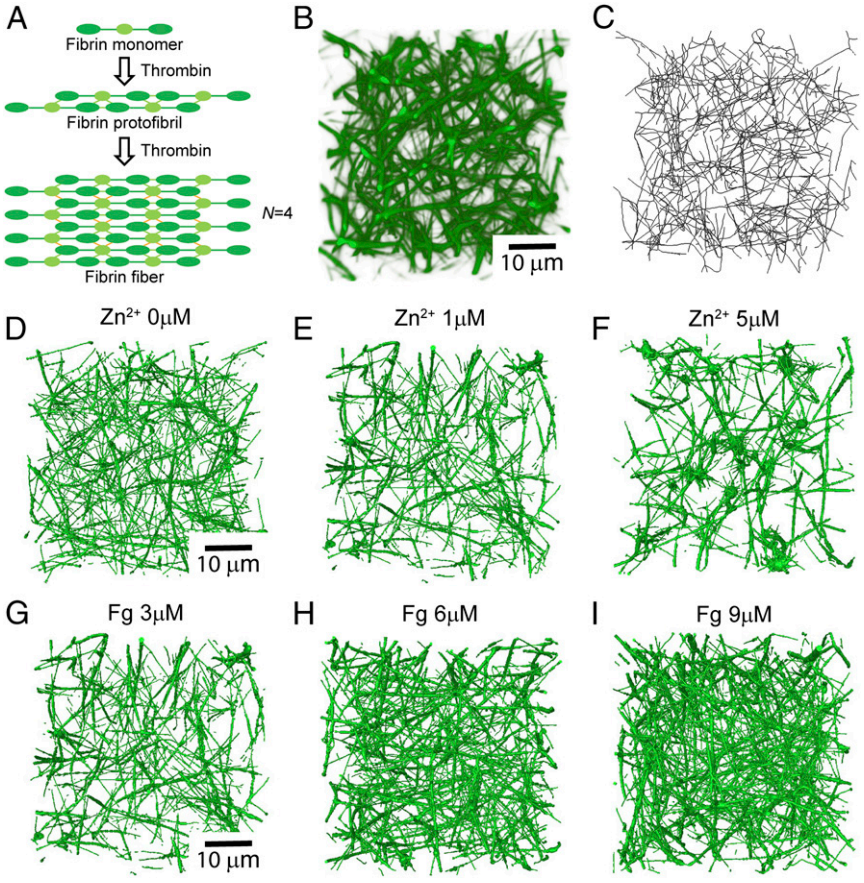

Fig. 1. Morphology of fibrin networks obtained with confocal fluorescence microscopy. (*A*) The formation of a fibrin fiber. With thrombin, fibrin monomers are converted into a two-stranded protofibril. The protofibrils are further bundled in a parallel manner to form a fibrin fiber, with *N* indicating the number of protofibrils in a fiber. (*B*) Three-dimensional confocal image of a fibrin network formed with 9 μM fibrinogen and 3 μM Zn^{2+}. (Scale bar, 10 μm.) (*C*) Skeleton of a fibrin network formed with 9 μM fibrinogen and 3 μM Zn^{2+} obtained by skeletonizing the confocal images with Amira software. (*D*–*F*) Three-dimensional rendering of confocal images of fibrin networks formed with 3 μM fibrinogen and different Zn^{2+} concentrations. The Zn^{2+} concentrations are indicated above each image. As the Zn^{2+} concentration increases, the fibrinogen forms thicker fibers while the network becomes sparser. (Scale bar, 10 μm.) (*G*–*I*) Three-dimensional rendering of confocal images of fibrin networks formed with different fibrinogen (Fg) concentrations, each polymerized with 1 μM Zn^{2+}. The fibrinogen concentrations are indicated above each image. As the fibrinogen concentration increases, the line density of the network increases greatly, while the fiber radius increases only slightly. (Scale bar, 10 μm.)

to calculate the fiber radius, a, the fiber line density, ρ, which is defined as the sum of the contour lengths of all fibers per volume, and the mesh size, ξ, which is defined as the average distance between two neighboring fibers.

To examine the effect of Zn^{2+} on the network morphology of fibrin gels, we keep the fibrinogen concentration constant while varying the Zn^{2+} concentration. As the Zn^{2+} concentration increases, the fibrinogen forms thicker fibers while the network becomes more heterogeneous, as shown by the reconstructed 3D images of fibrin gels in Fig. 1 *D–F*. Meanwhile, the fiber radius, a, increases almost twofold when the Zn^{2+} concentration increases from 0 to 5 μM, as shown in Fig. 2*A*. As the fiber radius becomes larger, the fiber length must become shorter to conserve the volume of the fibrinogen; this is confirmed by the approximately fourfold decrease in fiber line density, ρ, as shown in Fig. 2*B*. As a result of volume conservation, the mesh size must become larger as the line density decreases, as shown in *SI Appendix*, Fig. S1. To better compare fibrin gels under different polymerization conditions, we also vary the fibrinogen concentration while keeping the Zn^{2+} concentration constant. As the fibrinogen concentration increases, the network becomes denser, as shown in Fig. 1 *G–I*. At a fixed Zn^{2+} concentration, increasing the fibrinogen concentration 4-fold leads to only a slight increase in fiber radius, of ∼1.2-fold, as shown in Fig. 2*A*; by contrast, the line density increases greatly, by ∼2- to 3-fold, as shown in Fig. 2*B*. These results suggest that Zn^{2+} can promote bundling and increase the fiber diameter, while the amount of fibrinogen affects only the fiber line density.

As a simple consistency check, we verify the concentration dependence of the mesh size: The fibrinogen concentration, c_{Fg}, is proportional to fiber volume fraction, $\Phi \sim a^2/\xi^2$, assuming that fiber length is of the same order as mesh size. As a result, the ratio of mesh size to fiber radius scales with the fibrinogen concentration as a $-1/2$ power law, $\xi/a \sim c_{Fg}^{-1/2}$, as shown in Fig. 2*C*.

To further understand the network structure under different polymerization conditions, we analyze the 3D confocal images to calculate network connectivity, Z, which is a measure of network constraint defined as the average number of fibers connected at any branch point. Assuming that we have a fully cross-linked network, higher connectivity indicates a more constrained network, which will deform in an affine fashion, while a less constrained network with lower connectivity will deform nonaffinely and exhibit local structural reorganization (27, 28). We calculate the network connectivity by averaging over all branch points. Surprisingly, the network connectivity of fibrin gels remains the same regardless of changing Zn^{2+} or fibrinogen concentrations, as shown in *SI Appendix*, Fig. S2. This result indicates that network topology is similar in all fibrin gels independent of polymerization conditions, suggesting that the topological structure of the network forms in a robust way.

Fibrin fibers are not randomly packed; instead, they consist of protofibrils that are bundled in a parallel manner, as shown in Fig. 1*A*. To further investigate this bundling inside the fibers, we calculate the number of protofibrils in each fibrin fiber, N, using line density, ρ, protofibril mass-to-length ratio, μ, fibrinogen concentration, c_{Fg}, with the relation $N = c_{Fg}/(\mu\rho)$. We find that increasing either fibrinogen or Zn^{2+} concentration will lead to a significantly larger number of protofibrils packed in each fiber, increasing by about an order of magnitude, as shown in Fig. 2*D*. This trend is consistent with values of N derived empirically from measurements of the network turbidity (29), with magnitudes within a factor of 1.5. A comparison of the results from both methods is shown in *SI Appendix*, Fig. S3. More interestingly, the number of protofibrils packed in each fiber increases with Zn^{2+} concentration roughly as a square-root scaling, by the relation $N \sim c_{Zn}^{0.4-0.5}$, as shown in *SI Appendix*, Fig. S4.

Linear Rheology of Fibrin Networks. Based on the dramatically changed network morphology, and especially the large bundles observed in our networks, we expect a corresponding change in network mechanics. In our studies, up to a thousand or more protofibrils can bundle into a single fiber, yet it remains unclear how such a large degree of bundling will change the mechanical properties of the fibrin

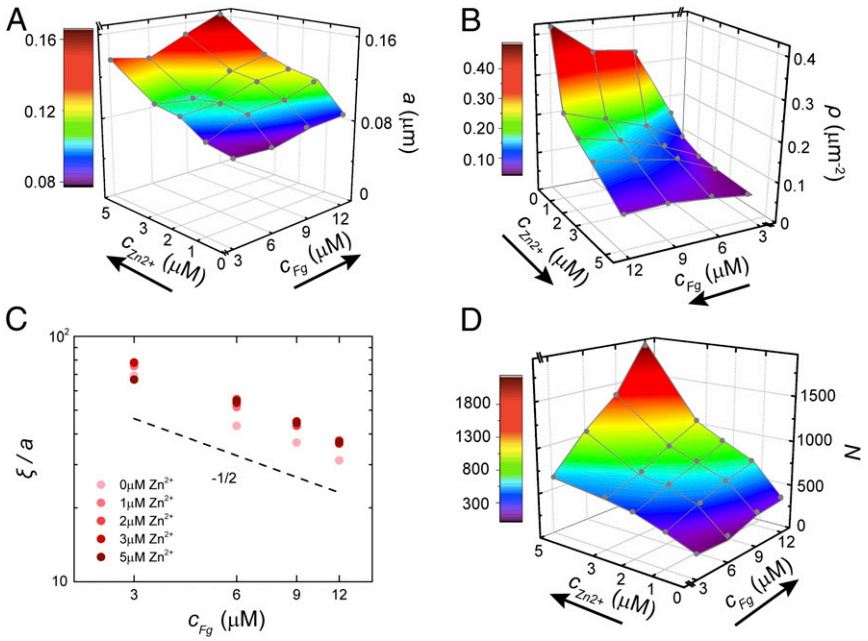

Fig. 2. Quantification of fibrin network structure. Reconstructed 3D confocal images of fibrin networks are quantified by the following: (*A*) radius of fibrin fiber, a, is plotted as a function of fibrinogen concentration, c_{Fg}, and Zn^{2+} concentration, $c_{Zn^{2+}}$. (*B*) Fiber line density, ρ, is plotted as a function of fibrinogen concentration, c_{Fg}, and Zn^{2+} concentration, $c_{Zn^{2+}}$. (*C*) Consistency check of fibrin networks. The mesh size, ξ, divided by the fiber radius, a, decreases with fibrinogen concentration according to a $-1/2$ power law, $\xi/a \sim c_{Fg}^{-1/2}$. (*D*) The average number of protofibrils in each fiber, N, is plotted as a function of the fibrinogen concentration, c_{Fg}, and Zn^{2+} concentration, $c_{Zn^{2+}}$.

networks. To quantify how Zn^{2+} changes the elasticity of fibrin gels and explore the elastic origin of such networks, we measure the rheological properties of the fibrin gels. We probe the rheological properties during the gel formation process by initiating polymerization of a fibrinogen solution, immediately loading it into a cone-and-plate geometry using a stress-controlled rheometer, and applying an oscillation controlled to be 0.5% shear strain at a frequency of 0.1 Hz. Here, the oscillation amplitude is well below the strain amplitude (10%) required to disrupt the formation of fibrin network; therefore, the network formation remains unperturbed (30). To further verify this, we repeat the experiment using a network that is allowed to form without any measurements. We compare the rheological properties of this inert network to those measured using a network subjected to oscillations during formation to follow its growth, where we apply a maximum strain amplitude of 0.5% at a frequency of 0.1 Hz. We find no obvious difference in both the storage and loss modulus between those two samples, as shown in *SI Appendix*, Fig. S5 *A* and *B*. As the fibrinogen polymerizes and forms a cross-linked network, both the storage modulus, G', and the loss modulus, G'', increase with time, and eventually reach plateaus once the network has fully polymerized, as shown in Fig. 3*A*. As both the oscillation amplitude (0.5% strain) and frequency (0.1 Hz) are small, the storage modulus measured at the plateau can represent the linear shear modulus, G_0. To further investigate the frequency dependence of the storage and loss moduli, a frequency sweep from 0.1 to 10 Hz is performed using the same strain of 0.5%. We find that the storage and loss moduli are essentially frequency independent below 1 Hz, and the storage modulus is an order of magnitude higher than the loss modulus, as shown in *SI Appendix*, Fig. S6 *A* and *B*. These results suggest that the Zn^{2+}-modified fibrin networks are solid-like, elastic networks.

To explore the nature of these Zn^{2+}-modified fibrin networks, and the origin of their elasticity, we investigate the scaling dependence of the linear shear modulus on fibrinogen and Zn^{2+} concentrations. The linear shear modulus increases approximately quadratically with the fibrinogen concentration from 3 to 12 μM for each Zn^{2+} concentration that we use. More precisely, G_0 increases with the fibrinogen concentration, c_{Fg}, as $G_0 \sim c_{Fg}^z$ with an exponent $z \cong 2.2$, as shown in Fig. 3*B*. This behavior is consistent with the scaling generally observed for semiflexible polymer networks originating from thermal fluctuations, as predicted by the semiflexible polymer model (14, 31, 32). This scaling is also consistent with the behavior of the elasticity of collagen networks, which are generally believed to be athermal, mechanical networks (33–35). Thus, from this scaling behavior alone, it is not possible to distinguish between thermal and athermal network elasticity. However, increasing the Zn^{2+} concentration leads to a clear decrease in the linear shear modulus, $G_0 \sim c_{Zn}^{-0.5}$, as shown in Fig. 3*C*. This decrease is highly unusual and quite unexpected; other divalent cations, such as Ca^{2+} or Mg^{2+}, lead to an increase in bundling and a similar modification of the network structure, but the linear modulus of fibrin gels increases (17, 36).

To investigate this anomalous behavior, we consider the implications of the strong bundling effect of Zn^{2+}, as shown in Fig. 1. One important effect is essentially structural or geometric: For a given fibrinogen concentration, bundling decreases the fiber line density, ρ_f, and increases the mesh size, ξ, as shown in Fig. 1. Thus, for a fiber bundle consisting of N protofibrils, ρ_f is related to the protofibril line density, ρ_{pf}, by the following relation:

$$\rho_f = \rho_{pf}/N. \quad [1]$$

The other effect of bundling is mechanical, in which bundling increases the bending rigidity κ of fibers. The strength of the

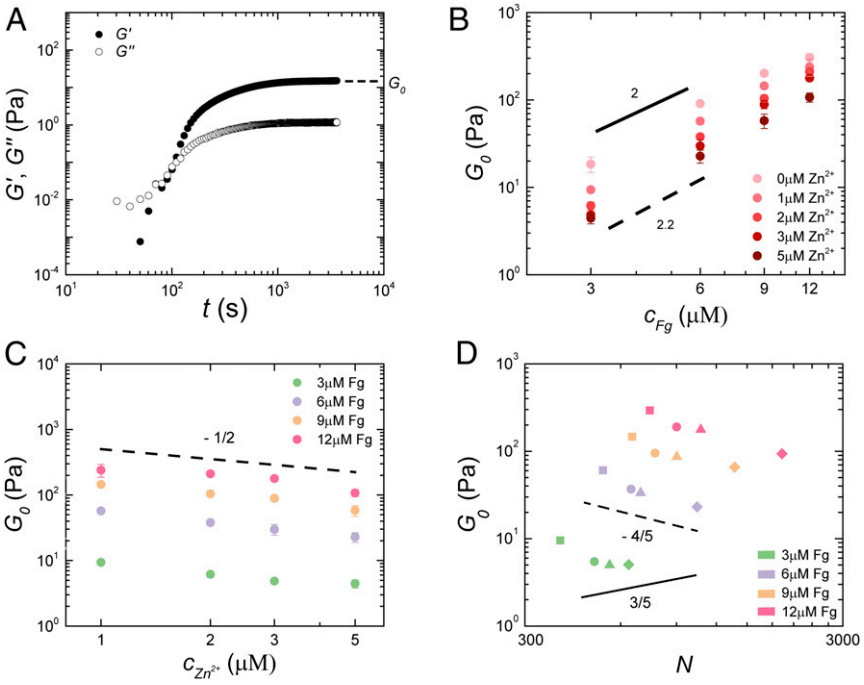

Fig. 3. Rheological properties of fibrin networks at low stress. (*A*) The storage modulus, G', and the loss modulus, G'', of a fibrin gel with 3 μM fibrinogen and 0 μM Zn^{2+} during polymerization process are plotted as a function of time, t. The storage modulus, G', increases with time and eventually reaches a plateau G_0 once the network has fully polymerized. (*B*) For each given Zn^{2+} concentration, the linear shear modulus of the fibrin network, G_0, scales with the fibrinogen concentration slightly larger than quadratic. (*C*) For each given fibrinogen concentration, the linear shear modulus of the fibrin network scales with Zn^{2+} concentration as G_0, $\sim c_{Zn^{2+}}^{-1/2}$. (*D*) For each given fibrinogen concentration, the linear shear modulus scales with the number of protofibrils as $G_0 \sim N^{-4/5}$ when Zn^{2+} concentration varies from 1 to 5 μM (1 μM Zn^{2+}, square; 2 μM Zn^{2+}, circle; 3 μM Zn^{2+}, triangle; 5 μM Zn^{2+}, diamond), indicating a tight coupling inside bundle. By contrast, for a loosely coupled bundle, the linear shear modulus would scale with the number of protofibrils as $G_0 \sim N^{3/5}$.

increase in bending rigidity, however, depends on the nature of the bundling. For so-called "tight bundles," in which the filaments in the bundle are tightly coupled in a lateral direction to prevent relative sliding, the bending rigidity κ is expected to increase quadratically with the number N of filaments in the bundle. By contrast, for "loose bundles," where individual fibers can slide laterally, the bending rigidity is simply additive, with $\kappa \sim N$. The bending rigidity κ is related to the persistence length l_p by the relation $l_p = \kappa/kT$, where k is the Boltzmann constant, and T is the temperature. Thus, we assume that

$$l_p^f = N^x * l_p^{pf}, \quad [2]$$

where l_p^f is the persistence length of the fibrin fiber, l_p^{pf} is the persistence length of the fibrin protofibril, and $x = 1$ or 2 for loose or tight bundling, respectively.

In the thermal affine model, the network shear modulus in the linear elastic regime, G_0, is as follows (31):

$$G_0 \sim \rho_f^{11/5} l_p^{f\ 7/5}. \quad [3]$$

Combining Eqs. **1**–**3** allows us to predict the effect of bundling on the linear shear modulus (13),

$$G_0 \sim \rho_{pf}^{11/5} N^{\frac{7x-11}{5}} l_p^{pf\ 7/5} \sim c_{Fg}^{11/5} N^{\frac{7x-11}{5}} l_p^{pf\ 7/5}. \quad [4]$$

Thus, for a given fibrinogen concentration, the linear shear modulus is predicted to increase with N for tight bundles and decrease with N for loose bundles. Our experiments are consistent with the latter case, where $G_0 \sim N^{-4/5}$, in good accord with the experimental data, as shown in Fig. 3*D*. A similar conclusion can also be drawn from the model for athermal fiber networks. For purely mechanical, athermal fiber networks, very general considerations would predict an approximate quadratic scaling of the shear modulus with concentration, for which

$$G_0 \sim E\varphi^2, \quad [5]$$

where φ is the volume fraction of polymer and E is the Young's modulus of the fibers (37–40). This model can also be applied to tightly bundled networks, for which the shear modulus is predicted to be independent of bundling. Since the elastic response is governed by bending, however, the shear modulus for loose bundles is predicted to decrease with N as $G_0 \sim 1/N$. Thus, our observations of a decreasing network stiffness with increased bundling by Zn^{2+} are clearly inconsistent with tightly bundled networks in either thermal or athermal limits. The decrease that we observe in Fig. 3*D* is, however, fully consistent with the mechanics of loosely bundled networks, regardless of the origin of the underlying mechanics.

The physical picture that arises from these results is that the role of Zn^{2+} is to cause the fibrin protofibrils to form thicker bundles when they assemble into long fibers. In the absence of Zn^{2+}, the fibrin protofibrils self-assemble into fibers that form the network structure. Upon addition of Zn^{2+}, the fibers further self-assemble into thicker bundles that form the network, leading to network coarsening with increasing Zn^{2+}. However, the fibers that form these bundles are loosely coupled to one another in the transverse direction. Because the fibers in the bundle are only loosely coupled, the bending rigidity of the bundles only increases linearly with the number of fibers. As a result, the mechanics of the full network reflect the thicker, but more sparse bundles, where the increase in rigidity of each bundle with increasing thickness is not sufficient to compensate for the increased sparseness of the network, and thus the network rigidity decreases as bundling increases. This directly reflects the weak transverse bonding. This behavior is in stark contrast with that of other divalent ions, which cause increasing stiffness with the increase of concentration as the bundling increases, presumably reflecting a stronger transverse bonding.

Nonlinear Rheology of Fibrin Networks. The physical picture of the fibrin network that emerges from the study of its structure and corresponding linear elastic behavior is that of a complex and hierarchical network. Such a network should also exhibit a correspondingly complex stress dependence in its elastic response, with distinct elasticity in different stress regimes (14). An elucidation of this response would provide further insight into the nature and structure of the network. To explore the nonlinear response of Zn^{2+}-modified fibrin networks, we perform a prestress test to probe the elastic behavior under large stresses. Small-amplitude stress oscillations of amplitude $\delta\sigma = 0.1\sigma$ and frequency 0.1 Hz are superimposed on a steady shear stress of magnitude σ, which is gradually increased in a stepwise manner. The storage modulus at each shear stress is taken as the differential modulus, $K'(\sigma) = \delta\sigma/\delta\gamma$. When the fibrin network is subjected to steady-state shear stress, the differential modulus is nearly constant at small stress, reflecting linear behavior. However, the differential modulus increases substantially at large stress, as shown in Fig. 4*A*. Such stiffening is qualitatively similar to the behavior of a wide range of biopolymer networks (15, 32). We define a characteristic stress σ_c where the differential modulus increases to 50% larger than its linear value, representing the onset of the nonlinear rheological response of the network, as shown by the red dashed lines in Fig. 4*A*.

In the thermal affine model, the characteristic stress of the network, σ_c, is as follows (31):

$$\sigma_c \sim \rho_f^{9/5} \left(l_p^f\right)^{3/5}. \quad [6]$$

Combining Eqs. **1**, **2**, and **6** allows us to predict the effect of bundling on the characteristic stress,

$$\sigma_c \sim \rho_{pf}^{9/5} \left(l_p^{pf}\right)^{3/5} N^{\frac{3x-9}{5}}. \quad [7]$$

As the line density of fibrin protofibril, ρ_{pf}, is proportional to the fibrinogen concentration, c_{Fg}, we obtain the following:

$$\sigma_c \sim c_{Fg}^{9/5} \left(l_p^{pf}\right)^{3/5} N^{\frac{3x-9}{5}}. \quad [8]$$

The predicted dependence of characteristic stress on fibrinogen concentration is consistent with that measured, as shown in Fig. 4*B*. Correspondingly, the characteristic strain decreases with the fibrinogen concentration with an exponent of −2/5 for varying Zn^{2+} concentration, as shown in *SI Appendix*, Fig. S7. This is consistent with the predicted dependence of characteristic strain on c_{Fg}, as determined by dividing the characteristic stress, Eq. **8**, by the modulus, Eq. **4**. Moreover, with the addition of Zn^{2+}, the measured characteristic stress for c_{Fg} above 3 μM is also consistent with the predicted $\sim N^{-6/5}$ dependence for loose bundling, as shown in Fig. 4*C*. The weaker N dependence we observe at the lower fibrinogen concentration may be an indication of nonaffine behavior, for which no dependence on N is predicted (13, 41).

As a further test of the consistency with the predictions in Eqs. **4** and **8**, we note that for loose bundles ($x = 1$), $[G_0/c_{Fg}]^{3/2}$ is predicted to be proportional to σ_c, with a prefactor that is independent of both the fibrinogen concentration $c_{Fg} \sim \rho_{pf}$, as well as the bundle number N, but depends only on l_p^{pf}. More precisely, $[G_0/c_{Fg}]^{3/2}$ scales with σ_c through the relation $[G_0/c_{Fg}]^{3/2} \sim \sigma_c l_p^{pf\,\frac{3}{2}}$. Indeed,

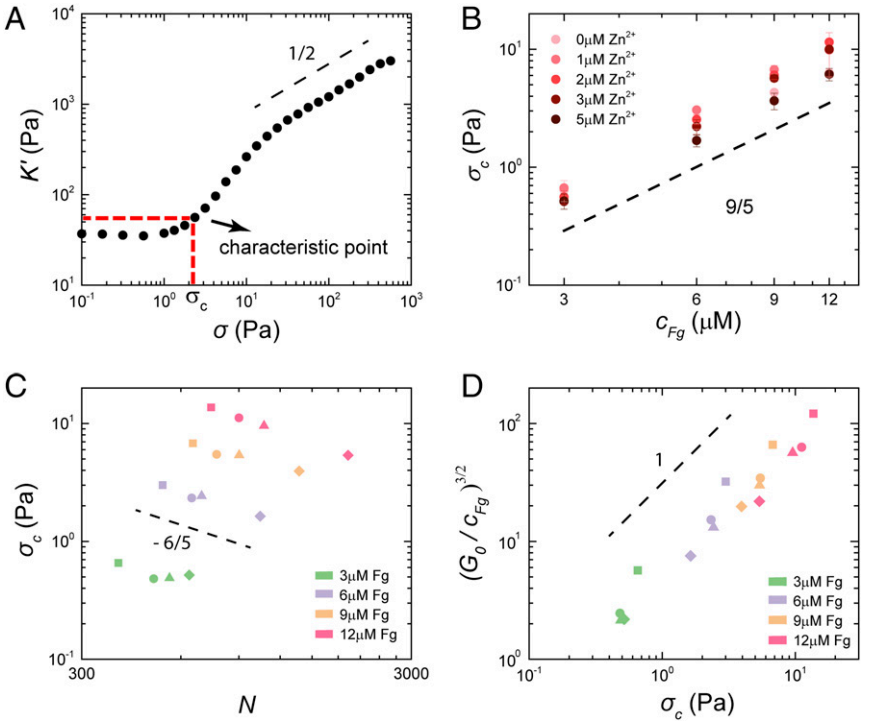

Fig. 4. Stress-stiffening transitions of fibrin networks. (*A*) The differential modulus, K', is plotted as a function of the prestress, σ. The characteristic stress at the onset of the stress stiffening is shown as σ_c. The fibrin network formed with 3 μM fibrinogen and 1 μM Zn^{2+} is shown as an example here. (*B*) The characteristic stress increases with the fibrinogen concentration as $\sigma c \sim c_{Fg}^{9/5}$ for various Zn^{2+} concentrations. (*C*) For each given fibrinogen concentration, the characteristic stress scales with the number of protofibrils as $\sigma c \sim N^{-6/5}$ when Zn^{2+} concentration varies from 1 to 5 μM (1 μM Zn^{2+}, square; 2 μM Zn^{2+}, circle; 3 μM Zn^{2+}, triangle; 5 μM Zn^{2+}, diamond). (*D*) For fibrin gels polymerized under different fibrinogen and Zn^{2+} concentrations, $[G_0/c_{Fg}]^{3/2}$ scales linearly with σ_c (1 μM Zn^{2+}, square; 2 μM Zn^{2+}, circle; 3 μM Zn^{2+}, triangle; 5 μM Zn^{2+}, diamond).

we find that the data fall onto the same line, in striking confirmation of this predicted scaling, as shown in Fig. 4*D*.

Since the affine model appears to capture most of the linear elastic properties and the characteristic stress of fibrin gels at higher fibrinogen concentrations, we normalize the applied stress,σ, by the characteristic stress, σ_c, and the differential modulus, K', by the linear modulus, G_0, to compare responses of the fibrin gels under different stresses. The resulting, normalized stiffness exhibits up to four distinct elastic regimes as a function of stress: (I) the first plateau regime, (II) the first stiffening regime,

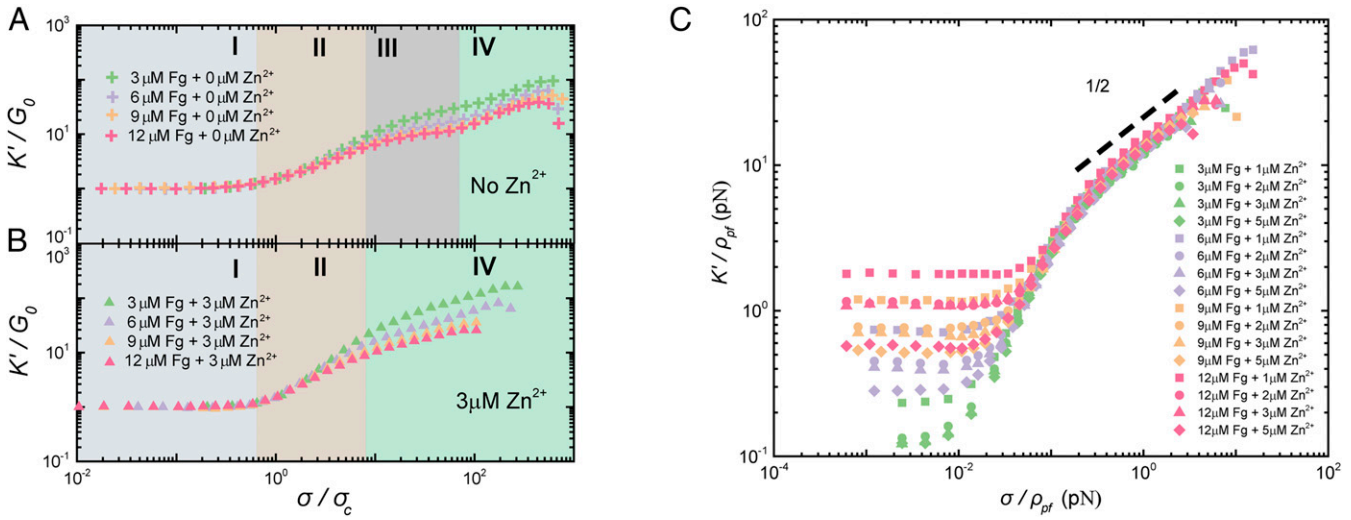

Fig. 5. Rheological properties of fibrin networks at high stress. The stress stiffening of fibrin networks obtained by normalizing the differential modulus and applied stress by the linear shear modulus and characteristic stress, respectively. (*A*) Fibrin networks with no Zn^{2+} show four regimes (I, II, III, and IV) during stress stiffening, clearly deviating from (*B*) fibrin networks with Zn^{2+}, which show three regimes (I, II, and IV). (*C*) The stress stiffening measured at different polymerization conditions, rescaled by the protofibril line density, ρ_{pf}. The data collapse onto a master curve at large stress (above 0.1 pN), indicating that the response of the network is a linear sum of the elastic response of individual protofibrils.

(III) the second plateau regime, and (IV) the second stiffening regime, as shown in Fig. 5*A*. Regime I exhibits a linear elastic response, with constant $K' = G_0$. Both the concentration and bundling dependence of this regime are consistent with an affine network response governed by thermal bending fluctuations. In regime II, the networks exhibit a stiffening response above the characteristic stress; this is also consistent with the behavior predicted by the affine model. In this regime, the increase of the stiffness over approximately one decade in stress is qualitatively consistent with that observed for other semiflexible polymer networks (15, 27, 32, 42, 43). As reported in prior experiments on fibrin gels, the networks show a transition at higher stress to a weaker stiffening response (13, 14). In the absence of Zn^{2+}, two distinct high-stress regimes (III and IV) can be identified for fibrinogen concentrations above 6 μM, as shown in Fig. 5*A*, while only a single high-stress regime is apparent for all samples with the addition of Zn^{2+}, as shown in Fig. 5*B*. This regime exhibits a robust power-law scaling $K' \sim \sigma^{1/2}$ over more than one decade, as shown for the sample with 3 μM fibrinogen and 1 μM Zn^{2+} in Fig. 4*A*. Moreover, this regime is consistent with a pure fibrin bundle stretching response, for which both the stiffness and stress are proportional to overall protofibril density ρ_{pf} (13); this is apparent when we scale both K' and σ by ρ_{pf}; all the data scale together very well and exhibit the $K'/\rho_{pf} \sim (\sigma/\rho_{pf})^{1/2}$ dependence expected for the high-stress regime, as shown in Fig. 5*C*.

The scaling exponent of 1/2 can be understood in simple terms. Neglecting polymer bending fluctuations that are responsible for the initial linear regime (I), the network should be unstable and floppy at low strain (27, 44, 45). This is because the connectivity or coordination number of the network is below the Maxwell (isostatic) threshold for a stable mechanical framework (46). Alternatively, since the linear modulus due to bending fluctuations (Eq. **4**) exhibits a stronger than linear dependence on fibrinogen concentration, this lack of mechanical stability can be visualized by taking the limit of low c_{Fg} in Fig. 5*C*, for which K'/ρ_{pf} vanishes. As even such a weakly connected network is strained beyond some threshold shear strain γ_c, it is no longer possible to deform it further without stretching. Hence, the stiffness can be expected to behave approximately as $K' = \delta\sigma/\delta\gamma \sim |\gamma - \gamma_c|$ (27, 47). Integrating this gives $\sigma \sim |\gamma - \gamma_c|^2$ and $K' \sim \sigma^{1/2}$. In contrast, high-concentration fibrin gels (6, 9, and 12 μM) formed without Zn^{2+} do not exhibit the same scaling across several stress regimes when their stiffening curves are normalized by protofibril line density ρ_{pf}, as shown in *SI Appendix*, Fig. S8. This suggests that their protofibrils are not loosely coupled, and therefore the contribution to high-stress mechanics is not linearly additive as occurs with the addition of Zn^{2+}. Further increasing the stress eventually results in the rupture of the fibrin gels, as shown by the dramatic drop in K' in Fig. 5*A*. For a fixed fibrinogen concentration, the rupture stress decreases only slightly with increasing Zn^{2+} concentration, as shown in *SI Appendix*, Fig. S9. Interestingly, for each value of Zn^{2+} concentration, the rupture stress exhibits a power-law dependence on the fibrinogen concentration, $\sigma_{rupture} \sim c_{Fg}^{7/5}$, as shown in *SI Appendix*, Fig. S10, which suggests that fibrin networks formed with or without Zn^{2+} share the same breaking mechanism.

The nonlinear data provide further insight into the rheological behavior of the fibrin networks; they are consistent with the behavior of thermal affine networks at low stresses, where the addition of Zn^{2+} induces bundling, but with the protofibrils only loosely coupled within the bundles, so the elastic modulus decreases. However, increased stress rapidly pulls out the thermal fluctuations of the protofibrils and then the elastic modulus results from stretching of the individual protofibrils, so the weak coupling is no longer material. This is reflected by the same scaling behavior of the elastic modulus at high stress regardless of Zn^{2+} and fibrinogen concentration.

Conclusions

Here, we have assembled highly bundled fibrin networks by adding Zn^{2+}, and we have explored the elastic origins of these networks at both low and high stress regimes. We show that, at low stresses, linear elasticity can be well characterized by the thermal affine model, in which the mechanical properties originate from pulling the thermal slack out of the network. By combining rheological measurements and confocal microscopy of the network morphology, we infer that fibrin networks formed in the presence of Zn^{2+} consist of bundles of fibrin protofibrils that are loosely coupled to one another; as a result, the magnitude of the elastic modulus decreases with increasing concentration of Zn^{2+}. At high stresses, the bending fluctuations are pulled out and the elasticity originates from stretching the individual protofibrils, resulting in a pronounced scaling behavior of all the data; in this case, the loose coupling is immaterial. Previous research has shown that Zn^{2+} binds to fibrinogen with high affinity, and that Zn^{2+} may increase fibrin fiber thickness at least in part by binding to the alpha-C regions of fibrinogen and promoting bundle formation (21). In this work, we show that these fibrin bundles are loosely coupled from a mechanical perspective, possibly resulting from the flexibility of the alpha-C regions of fibrinogen (48–50). It would be interesting to further measure the fibrin bundle mechanics and relate the mechanics with the protein structure in the future.

Our findings have important implications for understanding the origin of fibrin network mechanics, particularly the relationship between the fiber structure and its effect on network mechanics. These findings inform our understanding of the structure and physical mechanisms of abnormal clot formation in the presence of excess Zn^{2+} in the microenvironment within the clot. Furthermore, this understanding can be used in tissue engineering applications to design hierarchical fibrin scaffolds with multiscale control over the mechanical properties.

Materials and Methods

Polymerization of Fibrin Networks. To reconstitute the fibrin network, human α-thrombin (Enzyme Research Laboratories) and fibrinogen (FIB 1) (Enzyme Research Laboratories) are used. Fibrinogen is subjected to precipitation with 19% ammonium sulfate (Sigma-Aldrich) to ensure the highest integrity of the α-chains (51). Polymerization is performed in a Zn^{2+} buffering system (TcBS) containing 10 mM Tricine (Sigma-Aldrich), 150 mM NaCl (Sigma-Aldrich), pH 7.4, 2 mM $CaCl_2$ (Sigma-Aldrich), and 0.01% Tween 20 (Sigma-Aldrich) (21). Fibrinogen is incubated in TcBS buffer with different concentrations of $ZnCl_2$ (Sigma-Aldrich) for 5 min, and polymerization is initiated by adding 1 NIHU/mL α-thrombin.

Rheometry. Rheological properties of fibrin networks are measured with a stress-controlled rheometer (Hybrid DHR-3; TA Instrument). The prepolymer solution is prepared as described above. The prepolymer solution is then polymerized at 25 °C with a steel cone-plate geometry (40 mm diameter, 4°) whose temperature can be controlled using a Peltier device on the lower plate. Mineral oil (Sigma-Aldrich) is used to surround the sample to prevent drying. The storage and loss modulus are measured by applying an oscillatory strain with an amplitude of 0.5% at a frequency of 0.1 Hz while the network is polymerizing. Once the gel has fully polymerized, a frequency sweep (0.01 to 10 Hz) is performed using a strain amplitude of 0.5% to probe the frequency dependence of the storage and loss modulus. To probe the nonlinear response of fibrin networks at high stress, we use a differential measurement (52). Briefly, a small-amplitude stress oscillation of amplitude $\delta\sigma = 0.1\,\sigma$ and frequency 0.1 Hz is superimposed on a steady shear stress, σ, that is gradually increased in a stepwise manner. For each applied $\delta\sigma$, we measure the strain response, $\delta\gamma$. The complex differential modulus is given by $K^*(\sigma_0) = \delta\sigma/\delta\gamma$, which can be used to calculate the differential storage modulus, K', and the differential loss modulus, K''.

Confocal Microscopy Imaging. Fibrinogen is fluorescently labeled using TAMRA-SE (c1171; Thermo Fisher Scientific) following a previously reported protocol (53). Fluorescently labeled fibrinogen is then mixed with unlabeled fibrinogen at a ratio of 1:6 and polymerized between two 22-mm-diameter #1.5-thickness coverslips with a 1-mm-thick spacer. Samples are imaged with a confocal microscope (TCS-SP5; Leica Microsystems) equipped with a 63×/1.2 N.A. water immersion objective. Laser power is minimized and no obvious photobleaching is observed during the imaging process. Optical cross-sections are recorded at a *z*-axis interval of 0.1 μm to obtain 3D image stacks.

Image Analysis. To quantify the fibrin network morphology, Amira 6.0 software (Thermo Fisher Scientific) is used to analyze the image stacks. Image stacks are first deconvolved using the point spread function to enhance the signal-to-noise ratio and resolution, and then skeletonized with the Autoskeleton module to extract the network topology. The skeletonized image stacks are then processed with the Spatial Graph Statistics module to quantify the fiber radius, network connectivity, and line density of the fibrin networks.

To measure the mesh size of a fibrin network, each image stack is binarized using Otsu's threshold method. The mesh size is measured based on the binarized image stacks as described previously (54). Briefly, pixels with intensity above the threshold are considered to be part of a fibrin fiber; here, we call it "fiber pixel." The distance between the fiber pixels defines the fiber spacing *l*. The distribution of fiber spacing *l* is fitted into an exponential function $P(l) = P_0\exp(-l/\xi)$ with two independent fitting parameters: the scale parameter, P_0, and the mesh size, ξ. Due to the homogeneity in the *x* and *y* directions, only the fiber spacing along the *x* axis is used to calculate the mesh size.

Turbidity Measurement of Fibrin Networks. To calculate the number of protofibrils in each fiber, we measure the mass-to-length ratio of fibrin fibers in their hydrated state by turbidimetry. These measurements are performed using a Cary 60 UV-Vis spectrophotometer (Agilent Technologies). The prepolymer solution is prepared as described above. The prepolymer solution is then quickly transferred into a disposable cuvette and sealed with a cap at room temperature (25 °C). Once the sample has fully polymerized, optical density, *D*, is measured as a function of wavelength, λ, between 650 and 800 nm. Turbidity, τ, is calculated based on the following relation (55): $\tau = Dln(10)$. The mass-to-length ratio of the fibrin fiber, μ, can be further calculated by the following equation:

$$\tau\lambda^5 = 2\pi^3 C n_s \mu \left(\frac{dn}{dc}\right)^2 \frac{44}{15}\left(\lambda^2 - \frac{184}{154}\pi^2 a^2 n_s^2\right),$$

where τ is the turbidity, λ is the incident wavelength (in centimeters), μ is the mass-to-length ratio of the fibrin fiber (in daltons per centimeter), *a* is the fiber radius (in centimeters), *C* is the fibrinogen mass concentration (in grams per milliliter), and $n_s = 1.33$, $dn/dc = 0.17594\ \mathrm{cm^3 \cdot g^{-1}}$ (56). Given that individual fibrin protofibril has a mass-to-length ratio $\mu_0 = 1.44 \times 10^{11}$ Da/cm (57), the number of protofibrils in a fiber, *N*, is calculated as $N = \mu/\mu_0$.

Data Availability. All study data are included in the article and/or supporting information.

ACKNOWLEDGMENTS. We thank Jeffrey Weitz for motivating this work and for valuable discussions. We thank Jeffrey Weitz and Sara Henderson for generously providing the fibrinogen and thrombin. This work is supported by the NSF (Award DMR-1708729 and Award DMR-1826623) and the NSF through the Harvard University Materials Research Science and Engineering Center (Grant DMR-2011754) and the Center for Theoretical Biological Physics at Rice (Award PHY-2019745).

1. J. W. Weisel, R. I. Litvinov, Mechanisms of fibrin polymerization and clinical implications. *Blood* **121**, 1712–1719 (2013).
2. J. W. Weisel, Biophysics. Enigmas of blood clot elasticity. *Science* **320**, 456–457 (2008).
3. J. W. Weisel, R. I. Litvinov, "Fibrin formation, structure and properties" in *Fibrous Proteins: Structures and Mechanisms*, D. Parry, J. Squire, Eds. (Springer, 2017), pp. 405–456.
4. J. W. Weisel, Fibrinogen and fibrin. *Adv. Protein Chem.* **70**, 247–299 (2005).
5. P. A. Janmey, J. P. Winer, J. W. Weisel, Fibrin gels and their clinical and bioengineering applications. *J. R. Soc. Interface* **6**, 1–10 (2009).
6. A. Chandrashekar, G. Singh, Jonah Garry, N. Sikalas, N. Labropoulos, Mechanical and biochemical role of fibrin within a venous thrombus. *Eur. J. Vasc. Endovasc. Surg*. **55**, 417–424 (2018).
7. V. Tutwiler *et al*., Rupture of blood clots: Mechanics and pathophysiology. *Sci. Adv.* **6**, eabc0496 (2020).
8. Y. Qiu, D. R. Myers, W. A. Lam, The biophysics and mechanics of blood from a materials perspective. *Nat. Rev. Mater.* **4**, 294–311 (2019).
9. A. L. Fogelson, K. B. Neeves, Fluid mechanics of blood clot formation. *Annu. Rev. Fluid Mech.* **47**, 377–403 (2015).
10. A. Undas, R. A. Ariëns, Fibrin clot structure and function: A role in the pathophysiology of arterial and venous thromboembolic diseases. *Arterioscler. Thromb. Vasc. Biol.* **31**, e88–e99 (2011).
11. R. A. Clark, Fibrin and wound healing. *Ann. N. Y. Acad. Sci.* **936**, 355–367 (2001).
12. Y. Uchida, N. Yoshimoto, S. Murao, Cyclic fluctuations in coronary blood pressure and flow induced by coronary artery constriction. *Jpn. Heart J.* **16**, 454–464 (1975).
13. I. K. Piechocka *et al*., Multi-scale strain-stiffening of semiflexible bundle networks. *Soft Matter* **12**, 2145–2156 (2016).
14. I. K. Piechocka, R. G. Bacabac, M. Potters, F. C. Mackintosh, G. H. Koenderink, Structural hierarchy governs fibrin gel mechanics. *Biophys. J.* **98**, 2281–2289 (2010).
15. C. Storm, J. J. Pastore, F. C. MacKintosh, T. C. Lubensky, P. A. Janmey, Nonlinear elasticity in biological gels. *Nature* **435**, 191–194 (2005).
16. B. B. C. Lim, E. H. Lee, M. Sotomayor, K. Schulten, Molecular basis of fibrin clot elasticity. *Structure* **16**, 449–459 (2008).
17. G. Marx, Elasticity of fibrin and protofibrin gels is differentially modulated by calcium and zinc. *Thromb. Haemost.* **59**, 500–503 (1988).
18. S. J. Henderson *et al*., Zinc delays clot lysis by attenuating plasminogen activation and plasmin-mediated fibrin degradation. *Thromb. Haemost.* **113**, 1278–1288 (2015).
19. G. Marx, G. Korner, X. Mou, R. Gorodetsky, Packaging zinc, fibrinogen, and factor XIII in platelet α-granules. *J. Cell. Physiol.* **156**, 437–442 (1993).
20. A. I. S. Sobczak, F. A. Phoenix, S. J. Pitt, R. A. Ajjan, A. J. Stewart, Reduced plasma magnesium levels in type-1 diabetes associate with prothrombotic changes in fibrin clotting and fibrinolysis. *Thromb. Haemost.* **120**, 243–252 (2020).
21. S. J. Henderson *et al*., Zinc promotes clot stability by accelerating clot formation and modifying fibrin structure. *Thromb. Haemost.* **115**, 533–542 (2016).
22. K. A. McCall, C. Huang, C. A. Fierke, Function and mechanism of zinc metalloenzymes. *J. Nutr.* **130**, 1437S–1446S (2000).
23. B. L. Vallee, K. H. Falchuk, The biochemical basis of zinc physiology. *Physiol. Rev.* **73**, 79–118 (1993).
24. T. T. Vu, J. C. Fredenburgh, J. I. Weitz, Zinc: An important cofactor in haemostasis and thrombosis. *Thromb. Haemost.* **109**, 421–430 (2013).
25. E. Mammadova-Bach, A. Braun, Zinc homeostasis in platelet-related diseases. *Int. J. Mol. Sci.* **20**, 5258 (2019).
26. M. S. Rahman *et al*., "Morphological characterization of hydrogels" in *Cellulose-Based Superabsorbent Hydrogels*, M. I. H. Mondal, Ed. (Springer International Publishing, Cham, 2019), pp. 819–863.
27. C. P. Broedersz, F. C. MacKintosh, Modeling semiflexible polymer networks. *Rev. Mod. Phys.* **86**, 995–1036 (2014).
28. C. P. Broedersz, M. Sheinman, F. C. Mackintosh, Filament-length-controlled elasticity in 3D fiber networks. *Phys. Rev. Lett.* **108**, 078102 (2012).
29. C. Yeromonahos, B. Polack, F. Caton, Nanostructure of the fibrin clot. *Biophys. J.* **99**, 2018–2027 (2010).
30. S. Münster, L. M. Jawerth, B. Fabry, D. A. Weitz, Structure and mechanics of fibrin clots formed under mechanical perturbation. *J. Thromb. Haemost.* **11**, 557–560 (2013).
31. F. C. MacKintosh, J. Käs, P. A. Janmey, Elasticity of semiflexible biopolymer networks. *Phys. Rev. Lett.* **75**, 4425–4428 (1995).
32. M. L. Gardel *et al*., Elastic behavior of cross-linked and bundled actin networks. *Science* **304**, 1301–1305 (2004).
33. A. Sharma *et al*., Strain-controlled criticality governs the nonlinear mechanics of fibre networks. *Nat. Phys.* **12**, 584–587 (2016).
34. S. Motte, L. J. Kaufman, Strain stiffening in collagen I networks. *Biopolymers* **99**, 35–46 (2013).
35. K. A. Jansen *et al*., The role of network architecture in collagen mechanics. *Biophys. J.* **114**, 2665–2678 (2018).
36. M. Okada, B. Blombäck, Calcium and fibrin gel structure. *Thromb. Res.* **29**, 269–280 (1983).
37. A. J. Licup *et al*., Stress controls the mechanics of collagen networks. *Proc. Natl. Acad. Sci. U.S.A.* **112**, 9573–9578 (2015).
38. R. L. Satcher, Jr, C. F. Dewey, Jr, Theoretical estimates of mechanical properties of the endothelial cell cytoskeleton. *Biophys. J.* **71**, 109–118 (1996).
39. K. Kroy, E. Frey, Force-extension relation and plateau modulus for wormlike chains. *Phys. Rev. Lett.* **77**, 306–309 (1996).
40. L. J. Gibson, M. F. Ashby, *Cellular Solids: Structure and Properties* (Cambridge University Press, 1999).
41. A. J. Licup, A. Sharma, F. C. MacKintosh, Elastic regimes of subisostatic athermal fiber networks. *Phys. Rev. E* **93**, 012407 (2016).
42. Y. C. Lin *et al*., Origins of elasticity in intermediate filament networks. *Phys. Rev. Lett.* **104**, 058101 (2010).
43. R. H. Pritchard, Y. Y. S. Huang, E. M. Terentjev, Mechanics of biological networks: From the cell cytoskeleton to connective tissue. *Soft Matter* **10**, 1864–1884 (2014).
44. S. Alexander, Amorphous solids: Their structure, lattice dynamics and elasticity. *Phys. Rep.* **296**, 65–236 (1998).

45. M. Sheinman, C. P. Broedersz, F. C. MacKintosh, Nonlinear effective-medium theory of disordered spring networks. *Phys. Rev. E Stat. Nonlin. Soft Matter Phys.* **85**, 021801 (2012).
46. J. C. Maxwell, L. On the calculation of the equilibrium and stiffness of frames. *London Edinburgh Dublin Philos. Mag. J. Sci.* **27**, 294–299 (1864).
47. M. Wyart, H. Liang, A. Kabla, L. Mahadevan, Elasticity of floppy and stiff random networks. *Phys. Rev. Lett.* **101**, 215501 (2008).
48. J. W. Weisel, L. Medved, The structure and function of the alpha C domains of fibrinogen. *Ann. N. Y. Acad. Sci.* **936**, 312–327 (2001).
49. O. Klykov, C. van der Zwaan, A. J. R. Heck, A. B. Meijer, R. A. Scheltema, Missing regions within the molecular architecture of human fibrin clots structurally resolved by XL-MS and integrative structural modeling. *Proc. Natl. Acad. Sci. U.S.A.* **117**, 1976–1987 (2020).
50. G. Tsurupa *et al*., Structure, stability, and interaction of the fibrin(ogen) alphaC-domains. *Biochemistry* **48**, 12191–12201 (2009).
51. J. B. Walker, M. E. Nesheim, The molecular weights, mass distribution, chain composition, and structure of soluble fibrin degradation products released from a fibrin clot perfused with plasmin. *J. Biol. Chem.* **274**, 5201–5212 (1999).
52. Y. C. Lin, G. H. Koenderink, F. C. MacKintosh, D. A. Weitz, Viscoelastic properties of microtubule networks. *Macromolecules* **40**, 7714–7720 (2007).
53. L. M. Jawerth, "The mechanics of fibrin networks and their alterations by platelets," PhD thesis, Harvard University, Cambridge, MA (2013).
54. P. M. Bendix *et al*., A quantitative analysis of contractility in active cytoskeletal protein networks. *Biophys. J.* **94**, 3126–3136 (2008).
55. M. E. Carr Jr, J. Hermans, Size and density of fibrin fibers from turbidity. *Macromolecules* **11**, 46–50 (1978).
56. G. E. Perlmann, L. G. Longsworth, The specific refractive increment of some purified proteins. *J. Am. Chem. Soc.* **70**, 2719–2724 (1948).
57. M. De Spirito, G. Arcovito, M. Papi, M. Rocco, F. Ferri, Small-and wide-angle elastic light scattering study of fibrin structure. *J. Appl. Cryst.* **36**, 636–641 (2003).